Available online at www.sciencedirect.com

SCIENCE DIRECT®

Earth and Planetary Science Letters 237 (2005) 311–325

EPSL

www.elsevier.com/locate/epsl

Rock magnetic properties of uncultured magnetotactic bacteria

Yongxin Pan [a,b,*], Nikolai Petersen [b], Michael Winklhofer [b], Alfonso F. Davila [b], Qingsong Liu [a,c], Thomas Frederichs [d], Marianne Hanzlik [e], Rixiang Zhu [a]

[a] *Laboratory of Paleomagnetism, Geochronology and Biogeomagnetism (SKL-LE), Institute of Geology and Geophysics, Chinese Academy of Sciences, Beijing 100029, China*

[b] *Department of Earth and Environmental Science, Ludwig-Maximilians-University, Munich 80333, Germany*

[c] *Institute for Rock Magnetism, University of Minnesota, Minneapolis 55455, USA*

[d] *Department of Geosciences, University of Bremen, D-28334, Germany*

[e] *Department of Chemistry, Technical University of Munich, D-85748 Garching, Germany*

Received 25 February 2005; received in revised form 16 June 2005; accepted 24 June 2005
Available online 2 August 2005
Editor: V. Courtillot

Abstract

Understanding the magnetic properties of magnetite crystals (Fe_3O_4) produced by magnetotactic bacteria (MTBs) is of fundamental interest in fields of geosciences, biomineralization, fine particle magnetism, and planetary sciences. The database of bulk magnetic measurements on MTBs is, however, still too sparse to allow for generalizations due to difficulties in obtaining bacteria cells in sufficient quantities from natural environments, and the fact that only a few cultivable strains are available. Here we report the first series of magnetic measurements on two air-dried samples containing solely MTBs (wild-type cocci and *Magnetobacterium bavaricum*), which were directly isolated from carbonaceous lake sediments. Systematic rock magnetic studies show that: 1) the magnetosomes in cells are dominated by single-domain (SD) magnetite; 2) the samples have delta ratios δ_{FC}/δ_{ZFC} higher than 2; 3) the measured low-temperature remanence cycling curves as well as the first-order-reversal-curve (FORC) diagrams are significantly different to those measured on synthetic SD-magnetite samples; and 4) the Verwey transition temperature (T_v, ~100 K) of MTB cells is distinctly lower than that from stoichiometric magnetite (T_v, 120–125 K). Our results provide new insights on the magnetic properties of bacterial magnetite and advance the use of magnetic proxies for decoding the paleomagnetic signals of sediments containing bacterial magnetite.

Keywords: bacterial magnetite; uncultured magnetotactic bacteria; FORC diagram; Verwey transition; single domain

* Corresponding author. Laboratory of Paleomagnetism, Geochronology and Biogeomagnetism (SKL-LE), Institute of Geology and Geophysics, Chinese Academy of Sciences, Beijing 100029, China. Tel.: +86 10 62007913; fax: +86 10 62010846.

E-mail addresses: yxpan@mail.iggcas.ac.cn (Y. Pan), petersen@geophysik.uni-muenchen.de (N. Petersen), michael@geophysik.uni-muenchen.de (M. Winklhofer), fon@geophysik.uni-muenchen.de (A.F. Davila), liux0272@yahoo.com (Q. Liu), thofred@uni-bremen.de (T. Frederichs), marianne.hanzlik@ch.tum.de (M. Hanzlik), rxzhu@mail.igcas.ac.cn (R. Zhu).

0012-821X/$ - see front matter © 2005 Elsevier B.V. All rights reserved.
doi:10.1016/j.epsl.2005.06.029

1. Introduction

Magnetotactic bacteria (MTBs) are a diverse group of motile, aquatic bacteria including coccoid, rod-shaped, vibrioid, spririlla and multicellular forms that orient and migrate along the geomagnetic field. Hallmarks of the MTBs are intracellular magnetosomes, which are commonly magnetite (Fe_3O_4), and occasionally greigite (Fe_3S_4) crystals enveloped in a membrane structure. Magnetosomes are characterised by narrow grain-size distributions (30–120 nm), distinct species-specific crystal morphology, chemical purity, and arrangement in single or multiple linear chains (e.g. [1]). The magnetic properties of magnetosomes are of great interest for a number of reasons: (1) fossil magnetosomes can significantly contribute to the magnetic properties of sediments and soils in environments ranging from anoxic to oxic (e.g. [2–6]); (2) these nano-particles are novel sources for fundamental studies in fine-grain magnetism, magnetic materials and medical applications [7,8]; (3) the biological mechanisms underlying the magnetosome formation provide unique opportunities to uncover biomineralization in organisms [9,10]; and (4) fossil magnetosome chains have been proposed as suitable biomarkers for the presence of life on Earth and other planets (e.g., [11]).

In previous rock-magnetic studies on freeze-dried cells and isolated magnetosome chains of cultured *Magnetospirillum magnetotacticum* (formerly *Aquaspirillum magnetotacticum*), Moskowitz et al. [12,13] found strong chain–chain magnetic interactions after removal of the cellular body and reported that the dispersed whole cells exhibit different magnetic properties from those of synthetic, dispersed magnetite particles of comparable grain size. In these studies, the authors found that the different ratio of remanence loss at the Verwey transition temperature (T_v) between low temperature zero-field cooling (δ_{ZFC}) and field cooling (δ_{FC}) of the SIRM (saturation isothermal remanent magnetization) can be used as a useful parameter for the detection of magnetosome chains, e.g., delta ratio $\delta_{FC}/\delta_{ZFC}>2$ [13]. However, Carter-Stiglitz et al. [14] pointed out that this delta ratio is highly sensitive to the degree of oxidation of the particles, showing that there still exist ambiguities in the interpretation of the delta ratio. Moreover, the database of bulk magnetic measurements on MTBs is still too sparse to allow for generalizations, due to the fact that it is difficult to concentrate natural cells and so far only a few cultivable strains are available. Furthermore, although magnetic techniques have been proposed for rapidly diagnosing the presence of bacterial magnetite in bulk sediments, they have not been up to date validated on uncultured MTBs.

Here we report room- and low-temperature magnetic measurements on samples of air-dried, uncultured MTBs aiming to (1) characterize the magnetic properties of uncultured MTBs; and (2) validate the previously proposed rock-magnetic criteria for the identification of biogenic magnetite in bulk samples.

2. Sample preparation and magnetic measurements

2.1. MTB collection procedures

The MTB samples used in this study were collected from carbonaceous sediments of the Alpine foreland Lake Chiemsee (47°52′ N, 12°29′ E) in southeast Germany. Surface sediments from approximately 20 m water depth were scraped at the northern area of this lake in later October 2003 and stored in three 120 cm^3 glass aquariums at ambient temperature. Light microscopical examinations showed that the sediments host abundant MTBs, predominantly wild-type cocci and rod-shaped cells that are interpreted as *Magnetobacterium bavaricum* [15], and, to a lesser extent, a wild-type magnetotactic vibrio. Previous transmission electron microscopy (TEM) observations [16] revealed that the rod-shaped cell of *M. bavaricum* (Fig. 1a) could contain up to 1000 Fe_3O_4 magnetosomes arranged in 3–5 bundles of chains. The magnetosomes are bullet shaped, usually 100 nm long and 40 nm wide. On the other hand, the cocci (Fig. 1b) contain truncated hexahedral prisms of Fe_3O_4 magnetosomes with an average size of 110×70 nm, usually are arranged in two chains per cell. For our study, living cells were directly concentrated from the stored sediments using a Bacteriodrome in the Munich laboratory (a Leitz Laborlux D light microscope surrounded by two set of square coils orientated perpendicular to each other in the horizontal plane) following a standard procedure: first, a drop of fresh sediment was placed on a clean cover slide, and a drop of distilled water was

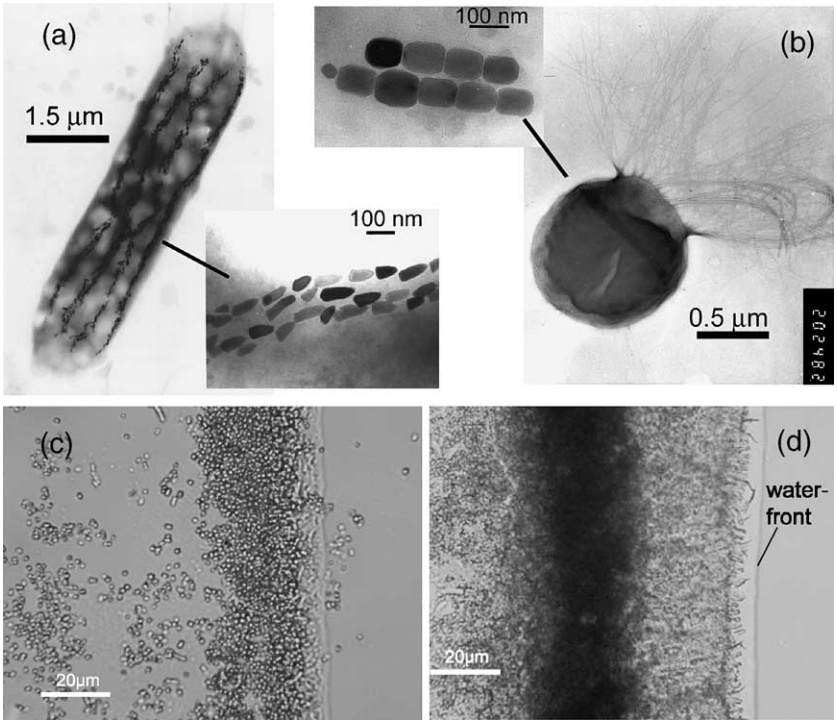

Fig. 1. Transmission electron microscopic micrographs of MTBs and their magnetosome crystal morphology, (a) *Magnetobacterium bavaricum* and (b) wild-type cocci, and micrographs showing the bacteria accumulation process (c–d) using a Bacteriodrome. Note that the applied field direction is from left to right, bacteria were concentrated at the right edge of the water droplet. The MTBs in (d) were accumulated by repeating the enrichment procedure many times.

added next to the sediment. A controlled weak magnetic field (0.1–0.4 mT) was applied so that the north-seeking bacteria would swim out of the sediment and into the water drop, eventually collecting at the water-front (Fig. 1c, d). The enrichment was carried out from January to early March 2004 until the concentration of cells sufficed for their magnetic characterization. Cells were air-dried at ambient temperature and stored in closure after each enrichment procedure to prevent environmental contamination. We successfully concentrated two pure MTB samples, named P2 and P3 (the preparation of the latter started in February), containing millions of cells in a very small area, $\sim 4 \times 8$ mm^2, suitable for magnetic measurements. The third sample (P1) was discarded due to sediment contamination during the preparation process. Observations in the light microscope showed that coccoid cells (Fig. 1c) were more abundant than *M. bavaricum* in samples P2 and P3. Room- and low-temperature magnetic measurements were carried out on both samples in March 2004.

2.2. Room-temperature remanent magnetizations, hysteresis and FORC diagram

We carried out room temperature measurements including the acquisition and demagnetization of the SIRM and anhysteretic remanent magnetization (ARM), hysteresis loops and the first-order reversal curve (FORC) analyses.

Stepwise SIRM acquisition and its demagnetization were performed in two approaches: (1) static field acquisition and back-field demagnetization on a Princeton Measurements Alternating Gradient Magnetometer AGM (Model MicroMag 2900); and (2) a pulse field IRM acquisition and alternating field (AF) demagnetization on a 2G Enterprises cryogenic magnetometer. The back-field demagnetization curve was transformed as $(1+\mathrm{IRM}(-\mathrm{H})/\mathrm{SIRM})/2$ to simplify comparison with the AF result.

ARM acquisition was obtained by a combination of a small steady bias field and a decaying AF field in two ways: (1) a weak steady DC field (0.05 mT)

combined with an increasing AF field (from 5 to 120 mT); and (2) a constant AF peak field of 100 mT with an increasing DC field (from 0.01 to 0.1 mT). Both were followed by stepwise AF demagnetization.

Hysteresis loops were measured using an Alternating Gradient Magnetometer (AGM, Model MicroMag 2900). To examine the domain state, we measured the saturation magnetization initial curves $M_{si}(B)$ before measuring the major hysteresis loop in a procedure proposed by [17]. First, apply field to maximum and then set it to zero to prepare the sample in the state of saturation remanence M_{rs}. In order to avoid overshooting to negative fields, fields to zero are set in 2 or 3 steps. Next, we measured initial curve plus hysteresis loop starting from this state. Hysteresis loops in different orientations were also measured for the anisotropy test.

The FORC method allows us to quantify the coercivity distribution and assess the role of magnetostatic interactions. Following [18], each FORC was measured by saturating the sample, decreasing the field to a value of H_a, and reversing the field sweep to the saturated state in a series of steps (H_b). This process was repeated for many values of H_a. The magnetization $M(H_a,H_b)$ was measured at each step and the mixed second derivative was taken to obtain the FORC distribution.

2.3. The delta ratio test

The delta ratio test [13] is based on two facts: (1) that the monoclinic phase of magnetite at low temperature has a larger magneto-crystalline anisotropy than the cubic phase and (2) that magnetosome chains have a pronounced shape anisotropy that favours the magnetization along the chain axis. As a result of (1), the magnetization of an individual magnetosome will take one of the monoclinic c-axes at $T<T_v$; as a consequence of (2), the c-axes nearest to the chain axis will be preferentially occupied. A strong magnetic field applied during cooling between 300 and 5 K, however, will outweigh the anisotropy due to the chain arrangement, such that those c-axes nearest to the field axis will be preferentially occupied. When the field is switched off at $T<T_v$ after the strong in field cooling (FC), the magnetization will be blocked in a metastable thermoremanence state, which is energetically less favourable than the remanence state induced in the zero field cooling (ZFC). After warming through the T_v the magneto-crystalline anisotropy tensor undergoes a symmetry change and the thermoremanence can be unblocked. Therefore, the presence of chains of magnetosomes in the samples will be revealed by the different thermal dependence of the magnetic remanences acquired after ZFC and FC.

The thermal dependence of SIRM between 5 and 300 K was measured using the Quantum Design Magnetic Property Measurement System (MPMS-7XL), a low-temperature superconducting quantum interference device (SQUID) magnetometer. The sensitivity of the magnetometer is 2×10^{-11} Am^2 and the residual field of the instrument is less than 0.2 mT. The SIRM given at 5 K in a strong field of 5 T ($SIRM_{5K}$) was measured in zero field at intervals of 2–5 K during the warming process,

Table 1
Comparison of the magnetic parameters (room-temperature experiments) of the uncultured MTBs, cultured MTBs and synthetic fine-grained magnetite particles

Samples		M_s (Am^2)	B_c (mT)	B_{cr} (mT)	M_{rs}/M_s	B_{cr}/B_c	R_{af} IRM (ARM)	MDF (mT) IRM (ARM)	ARM/SIRM
M-1[a]	Freeze-dried	–	26.7	27.6	0.53	1.02	0.62	32	0.11
M-2[a]	Extracted	–	3.7	16.6	0.41	4.49	0.21	9	0.005
MV1[b]	Wet cells	–	–	–	0.49	1.1	–	–	–
MS1[b]	Freeze-dried	–	–	–	0.44	1.1	–	–	–
P2[c]	Air-dried	6.7×10^{-8}	26.7	40	0.47	1.50	0.41(0.47)	43(49)	0.03
P3[c]	Air-dried	2.8×10^{-8}	33.4	45.5	0.51	1.36	0.39(0.44)	45(51)	0.02
Synthetic particles[d]	Cubic	–	21.3	30–40	0.28	1–2	–	28	–
	Acicular	–	38.4	50–60	0.4	1–2	–	43	–

[a]Moskowitz et al. [12]; [b]Moskowitz et al. [13]; [c]This study; [d]Dunlop [29]: cubic magnetite, 42 nm and acicular magnetite, 30×200 nm^2.

after samples were cooled from 300 to 5 K through the Verwey transition either in ZFC or in a FC of 5 T. The results of the measurements on samples P2 and P3 were corrected with the signal from the sample holder, and the delta ratio δ_{FC}/δ_{ZFC} was calculated after the definition of δ [13], i.e., $\delta = (M_{80K} - M_{150K})/M_{80K}$, where M_{80K} and M_{150K} is the remanent magnetization measured at 80 and 150 K, respectively.

2.4. Low-temperature cycling of SIRM

The cooling–warming cycling of SIRM was measured with the Quantum Design MPMS-7XL. The SIRM was given in a field of 5 T at 300 K ($SIRM_{300K}$), then in zero field cooled to 5 K and warmed back to 300 K. The remanence was continuously measured at intervals of 2–5 K during the cycling.

3. Results

Both P2 and P3 samples show nearly identical magnetic properties. Results are summarized in Tables 1 and 2.

3.1. IRM and ARM analyses

IRMs are saturated at a field of 100 mT, but as seen in Fig. 2a for sample P2, the pulse field curve shifts to higher fields compared to the DC field. A possible explanation for this phenomenon is related to the characteristic time response of the magnetite particles to the different magnetic treatments [13]. Because there is less time for the magnetosomes to respond to a pulse treatment, higher fields are required to achieve the same magnetization state obtained with the static field. A similar pattern is noted in the

Table 2
Comparison of the low-temperature demagnetization of saturation remanence of the whole cells, isolated magnetosomes of the cultured MTBs, the uncultured MTBs, extracellular magnetite and synthetic magnetic particles

Samples		T_v (K)	LTD-FC (%)	LTD-ZFC (%)	δ_{ZFC}	δ_{FC}	δ_{FC}/δ_{ZFC}
Whole cells							
MV1[a]	Wet	110	34	15	0.06	0.24	4.0
	Freeze-dried	101	36	–	0.04	0.19	4.8
MV2[a]	Wet	110	34		0.10	0.24	2.4
MS1[a]	Freeze-dried	101	35	15	0.06	0.16	2.7
AMB-1[b]	Freeze-dried	102	40	16	0.04	0.23	5.6
P2[c]	Air-dried	100	36	19	0.06	0.14	2.3
P3[c]	Air-dried	100	37	19	0.03	0.11	3.7
Mean		103.4	36.0	16.8	0.06	0.19	3.7
± SD		4.5	2.1	2.0	0.02	0.05	1.3
Isolated magnetosomes[a]			46	–	0.18	0.19	1.1
			–	–	0.21	0.22	1.0
			–	–	0.26	0.26	1.0
Extracellular magnetite							
GS-15[d]	668 h		–	–	0.09	0.15	1.6
	34 d				0.09	0.1	1.1
Synthetic particles							
Magnetite[a]	37 nm	120	68	–	0.38	0.48	1.3
	100 nm	120	80	–	0.52	0.67	1.3
	210 nm	120	90	–	0.82	0.86	1.0
	1000 nm	120	93	–	0.88	0.90	1.0
Maghemite[a]	–	–	15	–	0.02	0.03	1.1
Greigite[a]	–	–	19	–	0.05	0.05	0.9

[a]Moskowitz et al. [13]; [b]Weiss et al. [23]; [c]This study; [d]Vali et al. [32]. LTD_FC(ZFC) %=$(M_{20K} - M_{300K})/M_{20K} \times 100$. FC, field cooled; ZFC, zero-field cooled. T_v(K) is determined by the maximum of the dM/dT at the FC curves.

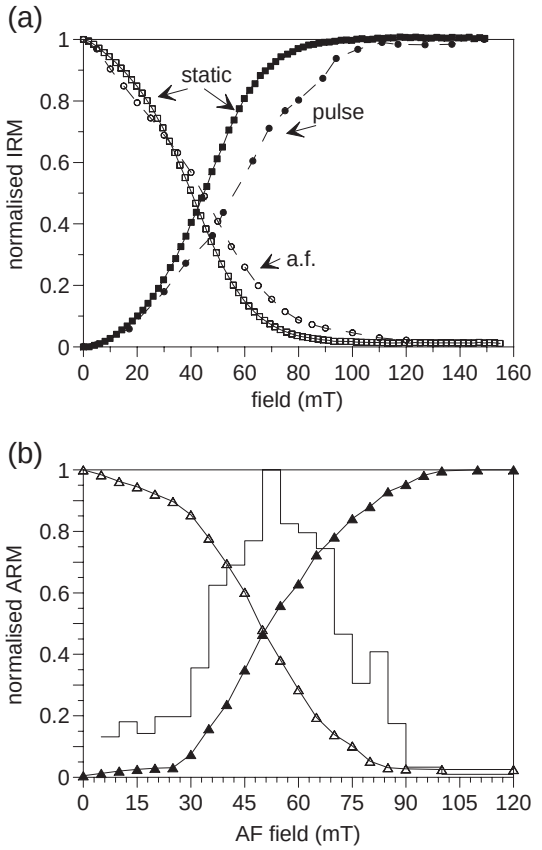

Fig. 2. Room-temperature magnetic measurements of sample P2. (a) Saturation remanent magnetization (SIRM) acquisitions by static and pulse fields, and demagnetization by AF and static approaches. (b) Anhysteretic remanent magnetization (ARM) acquisition in an increasing peak alternating field (filled triangles), AF demagnetization (open triangles) and the corresponding coercivity spectrum (line).

demagnetization curves. The median destructive fields (MDF), where the initial remanence is demagnetized by 50%, are 41 mT for the DC fields and 43 mT for AF demagnetization, respectively.

R-values of Wohlfarth–Cisowski test [19], which compare the IRM acquisition and demagnetization behavior, are R_{df}=0.45 (df refers to the DC field) and R_{af}= 0.41 for sample P2, suggesting moderate magnetic interactions. For sample P3, the respective values are MDF_{af}= 45 mT and R_{af}=0.39.

The ARM shows a shoulder in the demagnetization curve and a platform at the initial part of the acquisition curve, as obtained following approach (1) (Fig. 2b). The MDF by AF demagnetization obtained for sample P2 is ~49 mT and its *R*-value is 0.47. For sample P3, the corresponding values of MDF and *R*-value are 51 mT and 0.44. Both P2 and P3 samples show a linear dependence of the ARM with the DC-field up to 0.1 mT. The susceptibilities of ARM (χ_{arm}) are 177.2×10^{-5} SI.

3.2. Hysteresis

The saturation magnetization (M_s) of samples P2 and P3 (after superparamagnetic slope correction) is 6.7×10^{-8} Am^2 and 2.8×10^{-8} Am^2, respectively, suggesting that the relative amount of cells in the two samples is about 2.4:1. From the M_s values, we estimated an approximate number of cells in samples P2 and P3 of ~67 and ~28 millions, respectively (assuming the average magnetic moment of an individual MTB as 10^{-12} emu, [20]).

The hysteresis loops of samples P2 and P3 are characterized by their pot-bellied-shape (Fig. 3). The samples are saturated at a field of ~100 mT. The respective values of the coercive force (B_c) for samples P2 and P3 are 26.7 and 33.4 mT, while the remanence coercivity (B_{cr}) are 40 and 45.5 mT, the ratios of saturation remanence to saturation magnetization (M_{rs}/M_s) are 0.47 and 0.51, and the ratios of remanence coercivity to coercive force (B_{cr}/B_c) are 1.5 and 1.36, respectively. The hysteresis parameters indicate that the magnetosomes in the cells are SD magnetite, a result consistent with the IRM and ARM behaviors. This is further confirmed by the saturation initial curves measurements, i.e., the overlap between the $M_{si}(B)$ curves and the upper branches of loops (Fig. 3).

As samples were concentrated in a preferential direction during the accumulation (see Fig. 1c, d), a distribution anisotropy could be introduced by the sample preparation. To test this, we measured the sample P3 in six positions (three are shown in Fig. 3). From position (a) to (c), both the B_c and M_{rs}/M_s slightly increase. The higher values of B_c and M_{rs}/M_s in position (c) suggest a preferred chain orientation parallel to the swimming direction of cells.

3.3. The FORC diagram

We obtained the FORC diagrams of the P3 sample and a synthetic magnetite powder sample of comparable grain sizes for comparison. The magne-

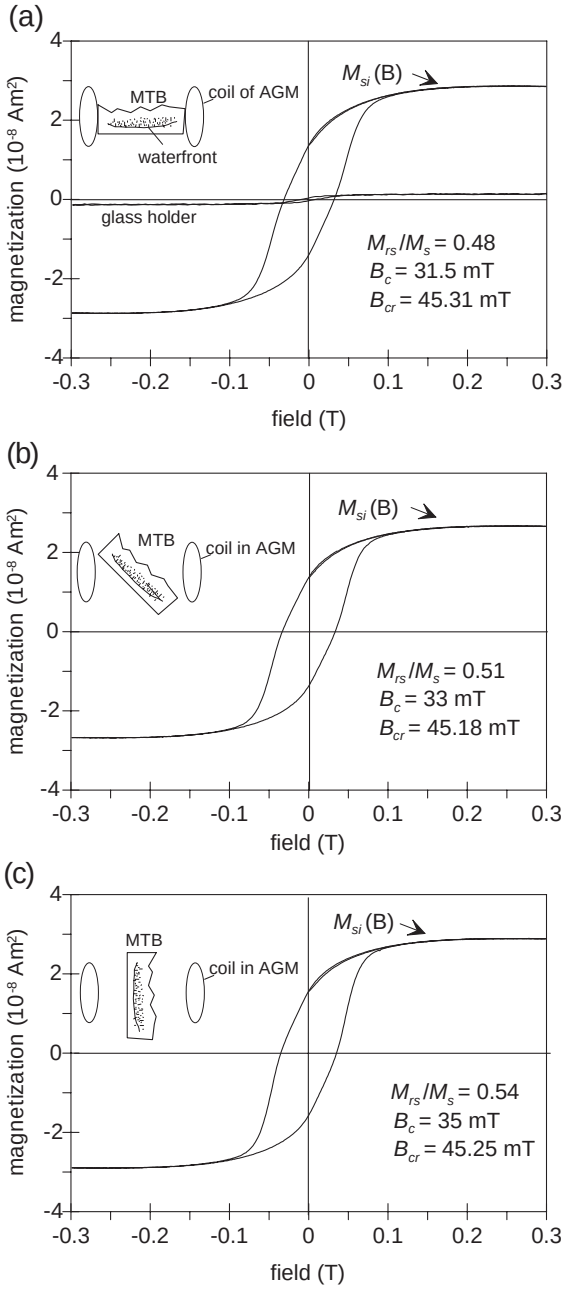

Fig. 3. Room-temperature hysteresis loops of sample P3 measured at different orientations. Note that the magnetosome chains are predominantly perpendicular to the waterfront, see text for details. AGM, alternating gradient magnetometer. M_s, M_{rs}, B_c and B_{cr} stand for the saturation remanence, saturation magnetization, coercive force and the remanence coercivity, respectively. The saturation initial curves $M_{si}(B)$ (thicker lines) are also shown. Hysteresis result of the glass holder is presented in (a), indicating negligible influence.

tite powder has a mean grain size of 50 nm. Its Verwey transition was determined as 120 K. The powder sample for the FORC measurement was not dispersed in a non-magnetic matrix, but just wrapped (in cling film) in order to maximize interactions effects.

The FORC distribution of the sample P3 (Fig. 4a) is concentrated along the $H_b=0$ axis with a smaller vertical spread compared to the FORC distribution of the SD powder sample (Fig. 4b). In both cases, the FORC distribution is slightly shifted towards negative H_b values, which we interpret as a mean-field effect. The characteristic interaction field in the MTB sample ($H_{b1/2}=6.3$ mT, defined as in the inset in Fig. 4a) is lower than that in the powder sample ($H_{b1/2}=8.3$ mT in the inset in Fig. 4b). The FORC distribution we obtained for the MTB sample is elongated along the H_c-axis (Fig. 4a). The coercivity distribution along the H_c axis has a major peak centered at $\mu=40$ mT and can be approximated by a normal distribution with a standard deviation of $\sigma=18$ mT. The coercivity distribution of the powder sample, on the other hand, followed a log-normal distribution ($\propto \exp(-\log(H_c/\mu)^2/(2\sigma^2))/H_c$, with $\mu=22$ mT and $\sigma=0.53$.

3.4. The delta ratio test

Fig. 5 shows results of the low-temperature magnetic measurements on P2 and P3 samples. The $SIRM_{5K}$ imparted at 5 K in an applied field of 5 T after FC treatment rapidly decay around the temperature intervals of 5–30 and 90–110 K (Fig. 5a,b). The latter is nearly depressed on the warming curves of the $SIRM_{5K}$ after ZFC treatments and only a small drop can be seen around 110 K. The delta ratio δ_{FC}/δ_{ZFC} are 2.3 and 3.7 for samples P2 and P3, respectively. This confirms that the threshold value ($\delta_{FC}/\delta_{ZFC}>2$) for bacterial magnetite of cultured MTB strains proposed by [13] also holds for the uncultured MTB cells.

3.5. Cycling curves of $SIRM_{300K}$ (300→5→300 K)

The zero-field cooling–warming cycling curves of $SIRM_{300K}$ are presented in Fig. 5c,d. Upon cooling curves (300→5 K), the remanence of the sample increases up to 130 K, then rapidly decreases between

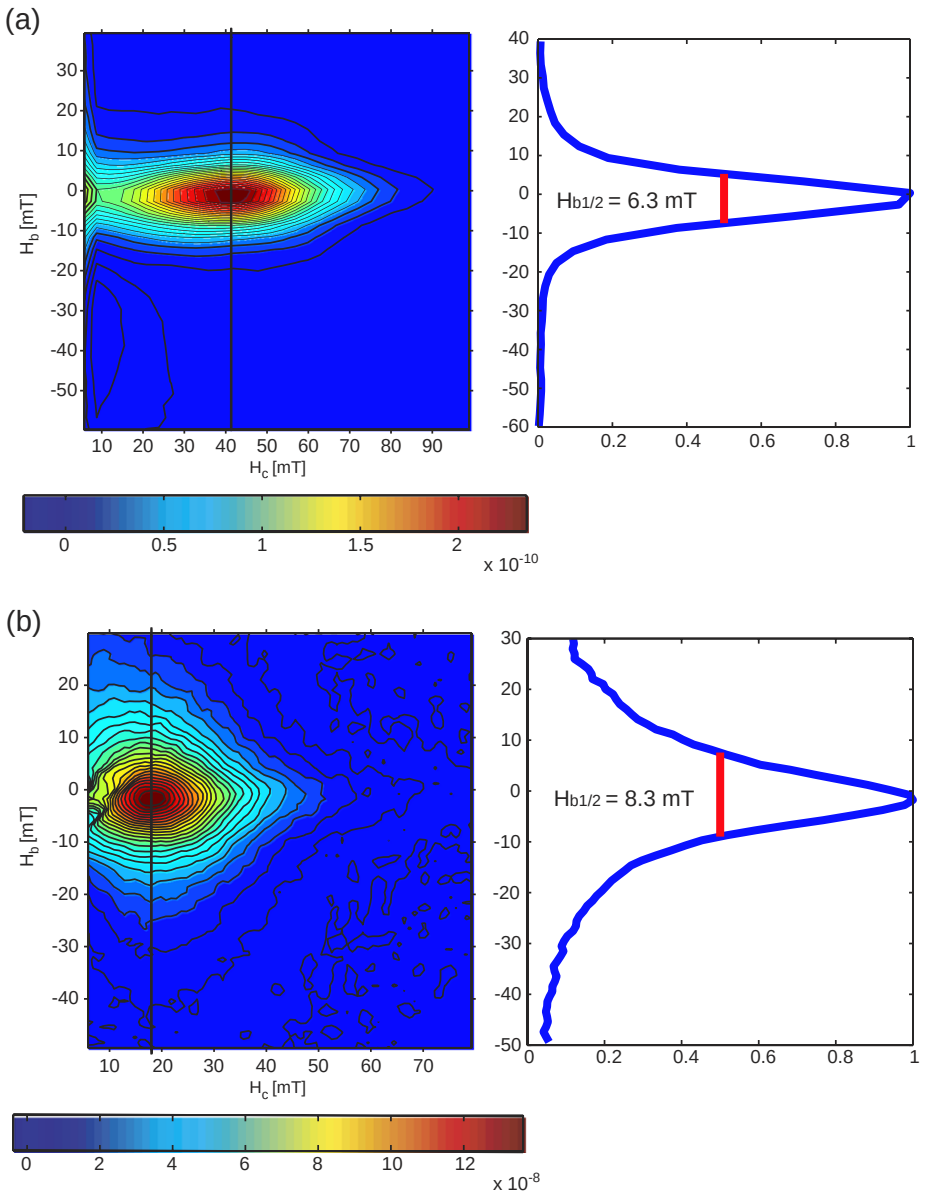

Fig. 4. FORC diagram of MTB sample P3 (a) and single-domain magnetite powder sample (b), both derived with a smoothing factor of 2. The FORC distribution of the MTB sample (a) is bimodal with a broad maximum centered at 42 mT and a sharper peak towards the H_c=0 axis. The latter is attributed to nascent magnetosomes as they typically occur at the chain ends. Insets in (a) and (b): Vertical profile through the high-coercivity peak of the distribution rendering a measure of the characteristic interaction strength, $H_{b1/2}$, defined as the value of the interaction field where the FORC distribution has reduced to half of its maximum value. Mean half-width field $H_{b1/2}$=6.3 mT at H_c=41.4 mT (a), mean $H_{b1/2}$=8.3 mT at H_c=17.8 mT (b).

100 and 70 K, and stays nearly constant down to 5 K, where the remanence gained is nearly 4% compared to the $SIRM_{300K}$. Upon warming curves (5→300 K), the remanence shows reversible behavior until 70–80 K with respect to the cooling curve, and partially increases below 100–130 K, then gradually decreases

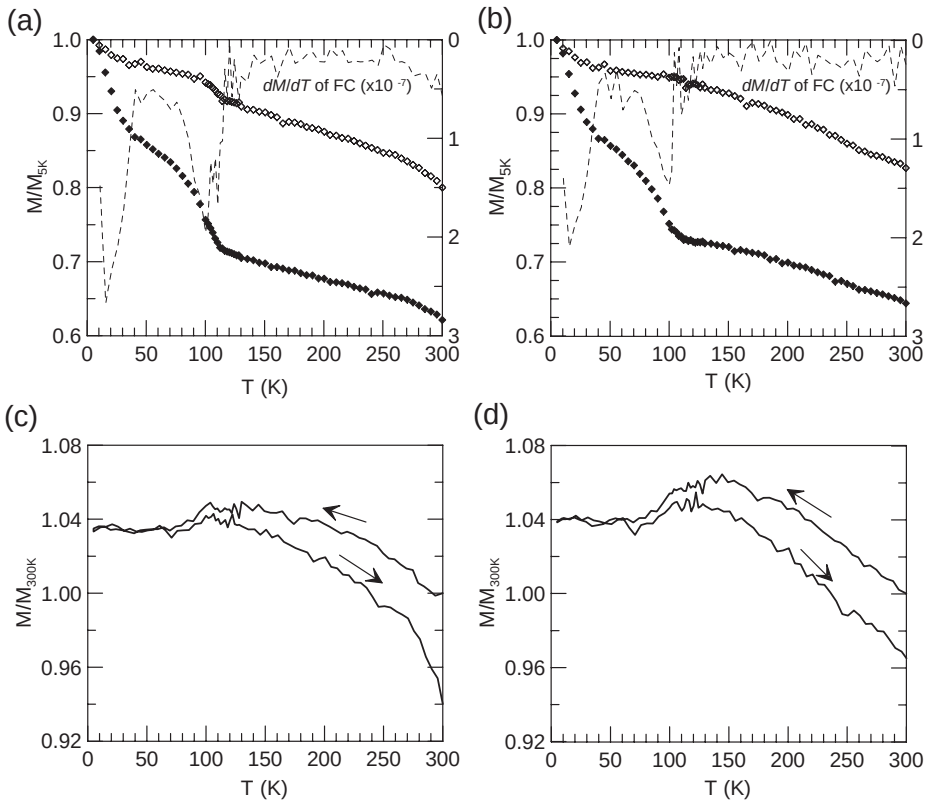

Fig. 5. Low-temperature magnetic measurements of the samples P2 (left) and P3 (right). (a) and (b), normalised $SIRM_{5K}$ warming curves after FC (filled diamond) and ZFC (outlined diamond) treatments, and the first derivatives of curves after FC (dashed line). (c) and (d), normalised $SIRM_{300K}$ cooling–warming cycling curves.

to 300 K. The remanence remaining at 300 K is 4–6% less than the initial value of $SIRM_{300K}$.

4. Discussion

4.1. Interpretations of the magnetic properties

The sample preparation technique used in this study enabled us to obtain samples containing solely uncultured MTBs. We obtained a mixture of two morphotypes of MTBs: wild-type cocci and large rod-shaped *M. bavaricum*. Direct visual observations confirmed that cocci are dominant in both P2 and P3 (see Fig. 1c).

The results of the room-temperature magnetic measurements indicate that the magnetosomes consist of SD magnetite. Evidences for that are (1) the shoulder seen in the demagnetization curve of ARM; (2) relative high B_c (~26–33 mT) and B_{cr} (~40–45 mT); (3) the low saturation magnetization field (<100 mT), the initial saturation curves and the broad pot-bellied shaped hysteresis loops; and (4) the closed pattern of the FORC diagram (see Figs. 2–4).

Our samples showed a small loss of remanence in the FC curves between 90 and 110 K, which are almost diminished in the ZFC curves (Fig. 5). We interpret this loss in remanence as a manifestation of the Verwey transition (T_v) for magnetite, albeit yielding values lower than expected (theoretical value ~120 K [21]). This low value of T_v suggests that the magnetite in samples P2 and P3 may have suffered a partial oxidation during sample preparation due to air-drying, resulting in the formation of maghemite rims on some grains [22]. Alternatively, the low value of T_v may represent an intrinsic magnetic nature of bacterial

magnetite (see discussion below). Causes for the remanence drop between 5 and 30 K in the curves after FC cooling are however unclear. We propose two explanations: (1) the paramagnetic behavior of growing magnetosomes just below the threshold of SD/SP, and/or (2) a decrease of the effective SD grain size due to partial oxidation.

The delta ratios δ_{FC}/δ_{ZFC} of samples P2 and P3 are greater than 2, thus the proposed criterion for the detection of magnetosome chains obtained for cultured cells ($\delta_{FC}/\delta_{ZFC}>2$) holds in our uncultured MTBs. As mentioned above, the delta ratio test relies on the chain arrangement of the magnetosomes, and the delta ratios obtained here suggest that most of magnetosomes in our samples have been preserved in chains. A predominance of disrupted chains (e.g., isolated magnetosomes) would yield values close to 1 [13]. It is still an open question as to whether chains of oxidized magnetosomes yield enhanced delta ratios as predicted from numerical modelling. While the delta ratio of an *Magnetospirillum magnetotacticum* MV-1 sample increased strongly from 1.55 to 4.8 after 3 years of aging [14], an *Magnetospirillum magnetotacticum* MS-1 sample had a ratio of 1.1 after 4 years of exposure to air [23]. On way to test this hypothesis is by measuring the two samples prepared following two different drying protocols (air-drying and freeze-drying) and compare their delta ratios. Because it is unpractical to obtain a sufficient number of uncultured cells from sediments by freeze-drying methods using our technique, it would be desirable to test the oxidation effect by applying both air-dried and freeze-dried preparation in a same cultured strain.

Özdemir et al. [24, Fig. 5] reported the cycling curve of the SIRM of a synthetic fine-grained magnetite sample (median particle size of 0.037 μm), showing a cooling curve almost flat between 300 and 150 K, and a remanence loss of c.a. 5% of the initial SIRM value. SIRM cooling and warming were reversible for the monoclinic phase in the range of 5–90 K, with all but 2% of the initial SIRM intensity being recovered at 5 K. Warming through the Verwey transition resulted in a remanence loss, with 85% of the initial SIRM remaining at 300 K. However, as seen in Fig. 5c, d, both P2 and P3 show significant differences: (1) Between the room temperature and the isotropic point T_i at 130 K, the SIRMs on both cooling and heating curves have reverse relationships with temperature. (2) At 5 K the SIRM increases by 4% compared to the initial SIRM. (3) When crossing T_v upon warming, the SIRM is partially recovered. (4) The SIRM remaining at 300 K is about 95% of the initial SIRM intensity. This intriguing contrast in the response of the MTB samples and the synthetic magnetite samples in the cooling–warming cycle may be related to the predominance of chain arrangements in the MTB samples. We plan further investigations (e.g., micromagnetic simulation) to verify this point. The MTB sample did not display an intensity jump on crossing T_v during cooling. One explanation is that when cooling through T_v, the sharp increases in coercivity will turn SD-PSD particles of magnetite from vortex state into flower state [25], thereby increasing the bulk remanence intensity.

4.2. Magnetostatic interaction

Magnetic interactions between grains strongly affect their magnetic properties [21]. Because our samples contain millions of dehydrated cells, the agglomeration of cells and shrinkage of the cell's membrane and cytoplasm could substantially enhance the particle and chain interactions, due to a decrease in the distance between magnetosomes and magnetosome chains. Grain interaction in SD case is the main reason for a finite ARM susceptibility [26,27]. For non-interacting, uniaxial SD particles, the R-value should be 0.5. When increasing interactions, it decreases. The R-values for our samples are 0.39–0.47, indicating moderate magnetostactic interactions. This is further confirmed by the ARM/IRM variation as a function of the applied DC fields (Fig. 6a). Previous studies on both natural and synthetic samples show that the ARM/SIRM gradually decreases when increasing the magnetic interaction [28,29]. Moreover, sample P2 has relatively lower B_c, B_{cr}, M_{rs}/M_s, and MDF values and the higher B_{cr}/B_c values than P3, probably due to the higher cell density. Supporting this idea is the fact that the sample of extracted magnetosomes of *A. magnetotacticum* (M-2) has much lower coercivity than that of the whole cell sample (M-1) (Fig. 6b).

The comparatively low interactions fields in the MTB sample can be rationalized as follows. The magnetite crystals within a magnetosome chain are fairly regularly arranged, giving rise to relatively uniform intra-chain interaction fields of some 60 mT

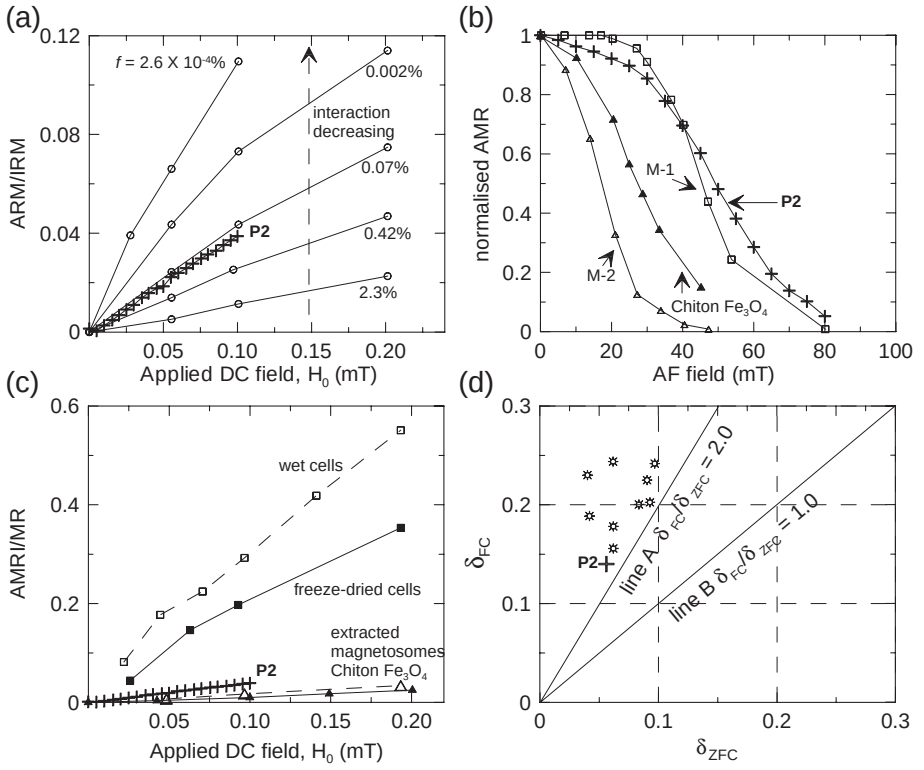

Fig. 6. Comparisons of the sample P2 (cross, this study) with other biogenic magnetite and inorganic magnetite. (a) The field dependence of ARM/IRM of the P2 comparison with samples containing dispersed magnetite in different concentrations [28]. (b) ARM remanence spectra of the P2 comparing with the cultured *A. magnetotacticum* (M-1, freeze-dried cells; M-2, extracted magnetosome chains) [12,13], and chiton magnetite [19]. (c) The field dependence of ARM/IRM of the P2 comparing with the cultured *A. magnetotacticum* (MV1, wet cells; freeze-dried cells; extracted magnetosome chains) [12,13] and chiton magnetite [19]. (d) A plot of δ_{FC} versus δ_{ZFC} for the whole cells of MTBs.

(except at the chain ends). On the other hand, the interaction fields in the FORC diagram barely exceed 20 mT, which is well below the intra-chain interaction field for magnetosomes. The dominating interactions picked up by the FORC diagram are therefore chain–chain and cell–cell interactions rather than intra-chain interactions. In other words, a chain of magnetosomes behaves as a single elongated particle (with uniaxial anisotropy) and switches as a unit, as demonstrated by remanence measurements on individual magnetic bacteria [30]. Thus, we may attribute the microcoercivity distribution to switching events where the whole chain polarity is reversed. Interestingly, the MTB sample shows a region with negative values of the FORC distribution whilst the magnetite powder sample does not, although both are dominated by uniaxial symmetry as inferred from the respective major hysteresis loops. Micromagnetic modelling [31] predicts such negative regions for randomly oriented SD particles with uniaxial symmetry. From our modelling of uniaxial Stoner–Wohlfarth particles, we would expect to see the negative region for the SD powder sample centered about $(H_b, H_c)=(-15, 5)$, that is, along the 45° line from $(H_b, H_c)=(-20, 0)$ to $(H_b, H_c)=(0,20)$. That region, however, is encroached by the large spread of the positive-valued FORC distribution, which thus veils the negative region.

4.3. Comparison with cultured MTBs and inorganic magnetites

The development of effective rock magnetic criteria for identifying bacterial magnetite in sediments depends heavily on our understanding of the specific properties of bacterial magnetite and the changes of these properties due to natural processes. It is there-

fore interesting to compare the results presented here with data found in the literature. Up to this day, the previous studies of the magnetic properties of bacterial magnetite have focused on cultured strains, which allow for a rapid sample preparation and characterization. In these studies, the samples were freeze-dried to avoid deterioration of the magnetic material. On the contrary, the preparation of our samples lasted between 1 and 2 months and the cells were air-dried at ambient temperature. Hence, caution should be taken when comparing our results with previous works as some difference may be due to the different protocols followed in sample preparation. On the other hand, our samples may reflect more closely the transformation processes that bacterial magnetite undergo in natural environments.

As can be seen in Table 1, our samples have larger values of B_{cr} and MDF than that of freeze-dried whole cells (M-1) and isolated magnetosomes (M-2) of *M. magnetotacticum* [12]. The ARM coercivity spectrum of sample P2 is comparable to the freeze-dried M-1, but higher than that of chiton magnetite and extracted magnetosome M-2 (Fig. 6b). These parameters do not exhibit clear consistencies among biogenic particles, while they are indistinguishable from that of a synthetic SD magnetite samples [29] (see Table 1), suggesting that those parameters alone cannot pinpoint the biogenic origin of the magnetite particles.

A comparison of the DC field dependences of ARM/SIRM with other bacterial magnetite particles (Fig. 6c) shows that the linear trend observed in the P2 sample at weak DC field is very similar to that of Chiton magnetite [19] and extracted magnetosomes [13], but well below the curves of wet cells and freeze-dried cells, which are non-linear up to field intensity of 1.5 mT [13]. These discrepancies could be caused by magnetic interaction effects (see 4.2), grain shape anisotropy (elongated magnetosomes in *M. bavaricum*) in our samples, and/or other discrepancies between bacterial species.

Importantly, whole cell samples of both uncultured (wild-type cocci and *M. bavaricum*) and cultured bacteria (strain MV, *M. magnetotacticum* MS-1, and *M. magneticum* AMB-1) have delta ratios greater than 2 (Table 2 and Fig. 6d), regardless of the preparation method (e.g. wet, freeze- or air-dried). This strongly confirms the assumption that intact chain arrangements lead to high delta ratios [13]. The extracted magnetosomes (disrupted chains) and SD magnetite induced by *Geobacter metallireducens* GS-15 (non-chain arrangement), on the other hand, have delta ratios less than 1.6 (Table 2). We have therefore validated for the first time the delta ratio test with naturally occurring populations of MTBs. The method thus stands as a resourceful tool for the identification of biogenic magnetite.

The average δ_{ZFC} and δ_{FC} values for whole cells, isolated magnetosomes, and extracellular magnetites (SD) produced by GS-15 cultured in low-CO_2 concentration [32], fall between ~0.1 and 0.3, which are distinctly lower than that of inorganic stoichiometric magnetite (including SD magnetite) and extracellularly-produced magnetite produced by GS-15 cultured in high-CO_2 concentrations, but higher than δ_{FC} of greigite and maghemite (Table 2 and Fig. 7). This suggests that the δ_{FC} can be used as a first indicator of bacterial SD magnetite. However, caution should be taken because δ_{FC} of nonstoichiometric (oxidised) inorganic magnetite may fall into the same range [34].

Another significant feature in Table 2 is that all whole cell samples show a distinctly low T_v between 100 and 110 K, regardless of species and preparation methods. Moskowitz et al. [13] first reported the $T_v \approx 100$ K for the wet and freeze-dried *Magnetospirillum magnetotacticum* strains MV1, MV2 and MS1. Recently, Weiss et al. [23] observed the Verwey transition at 102 ± 4 K for freeze-dried strains *Magnetospirillum magnetotacticum* strain 'AMB-1. Our samples show a $T_v \approx 100$ K. The low values of T_v may be interpreted as an intrinsic property of bacterial magnetite or as a result of oxidation processes during sample preparation, which alter the magnetic properties of the particles. However, the later interpretation is less likely because oxidation effects on wet and freeze-dried cells should be insignificant.

4.4. Implications for paleomagnetism and environmental magnetism

MTBs are ubiquitous in a broad range of natural environments from marine to continental habitats. When MTBs die, magnetosomes can be preserved in sediments and become important carriers of stable natural remanent magnetization. However, the contribution of bacterial magnetite to the sediment's magnetic properties has proved difficult to assess. To begin

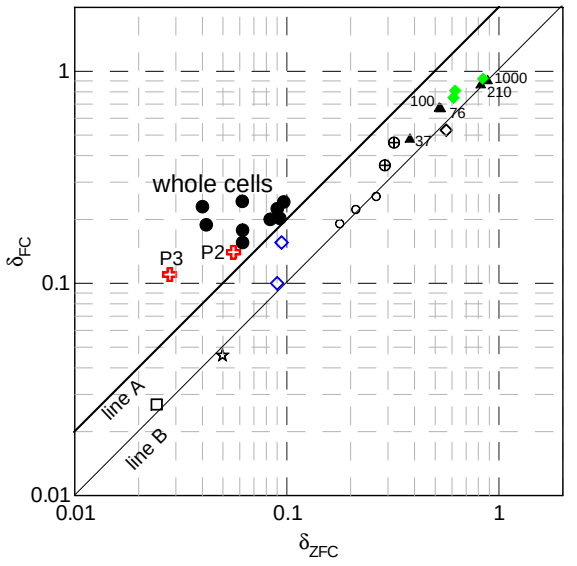

Fig. 7. Diagram of δ_{FC} versus δ_{ZFC} of the air-dried uncultured MTBs, P2 and P3, in comparison with other magnetite samples of biological and inorganic origins. Slopes of lines A and B are 2 and 1, respectively. Open crosses (red), this study; solid circles, wet or freeze-dried whole cells of strains MV1, MV2, MS1, AMB-1 (data from [13,23]); open circles, extracted magnetosomes [13]; blue open diamonds, extracellular magnetite produced by GS-15 cultured in low-CO_2 [32]; black open diamonds, extracellular magnetite produced by GS-15 cultured in CO_2-rich condition [13]; green solid diamonds, Martian meteorite ALH84001 [33]; solid triangles, inorganic magnetite (with grain size marked in nm) [13]; circles with crosses, carbonaceous sediments containing bacterial magnetite [6]; star and open square, greigite and maghemite [13], respectively. (For interpretation of the references to colour in this figure legend, the reader is referred to the web version of this article.)

with, the database on magnetic properties of uncultured MTBs is still sparse. Then it is not clear under which conditions magnetosome chains can be preserved as such and if they resist post-depositional alterations such as maghemitization (e.g. [22]) and diagenetic dissolution (e.g. [35,36]). Lastly, it is non-trivial to mathematically isolate the bacterial magnetite end-member component from mixtures of magnetic minerals of different origin and composition, despite a promising approach developed recently by Egli [37].

Pan et al. [6] recently investigated the magnetic properties of surface sediments in lake Chiemsee. The combination of magnetic and non-magnetic techniques (TEM and X-ray diffraction analyses) demonstrated the presence of bacterial magnetite in the topmost 5 cm of the sediment, in coexistence with coarser-grained detrital magnetite. The authors reported a strong similarity of the remanence coercivity spectra between bulk sediments and pure MTB samples, supporting the idea that bacterial magnetite can be a main magnetic component in the topmost few cm of the sediments [6, Fig. 10]. This biogenic component, however, rapidly disappeared in the sediment column leading to a significant change in the rock magnetic properties of the sediment. As seen in Fig. 7, the δ_{FC} values of bulk sediments fall between those of the inorganic magnetite and magnetosomes, suggesting an important contribution of the later to the bulk magnetic properties of the sediments. However, the bulk sediments containing MTBs failed to pass the delta ratio test. The low delta values were interpreted by [6] as being due to the presence of multidomain detrital magnetite, disrupted magnetosome chains and possibly incipient low-temperature oxidation of the bacterial magnetite. Hence, at the present state of knowledge, rock magnetic criteria alone cannot unravel the biogenic origin of magnetite particles in bulk sediment samples. The construction of more effective rock magnetic criteria for detection of bacterial magnetite in bulk sediments heavily depends on our understanding of differences between biogenic and inorganic magnetite, and more studies on both cultured and uncultured MTB species and the preservation state of the magnetosome chain arrangement in natural environments are necessary.

5. Conclusions

Based on the discussion above, the following conclusions can be drawn:

(1) Rock magnetic measurements of two bulk samples containing solely cells of wild-type cocci and *M. bavaricum* indicate that the magnetosomes are dominantly single-domain magnetite.
(2) The delta ratio test consistently yielded values greater than 2 (2.3 and 3.7), the threshold for magnetosome chains as first established in cultured MTB cells and is now confirmed for uncultured MTB cells. The method therefore stands as a resourceful tool for the identification of biogenic magnetite particles arranged in chains. Moreover, the δ_{FC} values (consistently

falling between 0.1 and 0.3) may also be used as an additional proxy for the detection of magnetosomes.

(3) Low-temperature SIRM cycling curves and first-order-reversal-curve (FORC) diagrams of the MTB samples differ significantly from the ones measured on SD-magnetite powder samples. The switching field distributions were found to obey a normal distribution in the MTB sample (mean at 40 mT) and a log-normal distribution in the powder sample (mean at 20 mT), respectively.

(4) The results from our bulk magnetic measurements (vertical spread in the FORC diagram; *R*-values slightly below 0.5; ARM versus the weak DC field intensity) indicate weak to moderate interaction fields in the MTB sample (despite high concentrations of MTB), which can be attributed to chain–chain or cell–cell interactions. The crystals in a chain act as a magnetic unit in rock magnetic bulk measurements (magnetic moment) and can therefore not be resolved as such. Spin-sensitive bulk methods such as EPR can be used as a complimentary tool to determine the mean strength of the interaction fields between crystals in a chain, as demonstrated in [23].

(5) Based on all available data, magnetosomes were found to undergo the Verwey transition at ~100 K, regardless of species and drying methods, which is distinctly lower than the Verwey temperature reported for stoichiometric magnetite (120–125 K). We advocate more research on this peculiarity, which may well turn out to be another diagnostic criterion of biogenic magnetite.

(6) Our samples have higher values of B_{cr} (~40–45 mT) and MDF (~43–45 mT), but lower values of ARM/SIRM compared to cultured MTB samples. This discrepancy is likely to be caused by different oxidation states, magnetic interactions or species-specific morphological properties of magnetosomes.

Acknowledgments

We thank K. Fabian and N. Nowaczyk for kind help with experiments. We are grateful to very constructive comments from three anonymous reviewers and A. Muxworthy for their suggestions, which help improve an earlier manuscript. This work was supported by NSFC grants 40325011 and 40221402, DFG grant Pe 173/13 and the Alexander von Humboldt Foundation (Germany).

References

[1] D.A. Bazylinski, A.J. Garratt-Reed, R.B. Frankel, Electron microscopic studies of magnetosomes in magnetotactic bacteria, Microsc. Res. Tech. 27 (1994) 389–401.

[2] N. Petersen, T.v. Dobeneck, H. Vali, Fossil bacterial magnetite in deep sea sediments from the South Atlantic Ocean, Nature 320 (1986) 611–615.

[3] S.B.R. Chang, J.L. Kirschvink, J.F. Stolz, Biogenic magnetite as a primary remanence carrier in limestone deposits, Phys. Earth Planet. Inter. 46 (1987) 289–303.

[4] J.W.E. Fassbinder, H. Stanjek, H. Vali, Occurrence of magnetic bacteria in soil, Nature 343 (1990) 161–163.

[5] Ø. Paasche, R. Løvlie, S.O. Dahl, J. Bakke, A. Nesje, Bacterial magnetite in lake sediments: late glacial to Holocene climate and sedimentary changes in northern Norway, Earth Planet. Sci. Lett. 223 (2004) 319–333.

[6] Y.X. Pan, N. Petersen, A.F. Davila, L.M. Zhang, M. Winklhofer, Q.S. Liu, M. Hanzlik, R.X. Zhu, The detection of bacterial magnetite in recent sediments of Lake Chiemsee (southern Germany), Earth Planet. Sci. Lett. 232 (2005) 109–123.

[7] S. Mann, Biomineralization: Principles and Concepts in Bioinorganic Materials Chemistry, Oxford University Press, Oxford, 2001, 210 pp.

[8] B. Yoza, M. Matsumoto, T. Matsunaga, DNA extraction using modified bacterial magnetic particles in the presence of amino silane compound, J. Biotechnol. 94 (2002) 217–224.

[9] R.B. Frankel, G.G. Papaefthymiou, R.P. Blakemore, W. O'Brien, Fe_3O_4 precipitation in magnetotactic bacteria, Biochim. Biophys. Acta 763 (1983) 147–159.

[10] D. Schüler, The biomineralization of magnetosomes in *Magnetospirillum gryphiswaldense*, Int. Microbiol. 5 (2002) 209–214.

[11] D.S. McKay, E.K. Gibson Jr., K.L. Thomas-Keprta, H. Vali, C.S. Komanek, S.J. Clemett, X.D.F. Chillier, C.R. Maechling, R.N. Zare, Search for past life on Mars: possible relic biogenic activity in Martian meteorite ALH84001, Science 273 (1996) 924–930.

[12] B.M. Moskowitz, R.B. Frankel, P. Flanders, R.P. Blakemore, B.B. Schwartz, Magnetic properties of magnetotactic bacteria, J. Magn. Magn. Mater. 73 (1988) 273–288.

[13] B.M. Moskowitz, R.B. Frankel, D.A. Bazylinski, Rock magnetic criteria for the detection of biogenic magnetite, Earth Planet. Sci. Lett. 120 (1993) 283–300.

[14] B. Carter-Stiglitz, B. Moskowitz, M. Jackson, More one the low-temperature magnetism of stable single domain magnetite: reversibility and non-stoichiometry, Geophys. Res. Lett. 31 (2004), doi:10.1029/2003GL019155 (L06606).

[15] N. Petersen, D.G. Weiss, H. Vali, Magnetic bacteria in lake sediments, in: Lowes, et al., (Eds.), Geomagnetism and Paleomagnetitism, Kluwer Academic Publishers, 1989, pp. 231–241.
[16] M. Hanzlik, M. Winklhofer, N. Petersen, Spatial arrangement of chains of magnetosomes in magnetotactic bacteria, Earth Planet. Sci. Lett. 145 (1996) 125–134.
[17] K. Fabian, Some additional parameters to estimate domain state from isothermal magnetization measurements, Earth Planet. Sci. Lett. 213 (2003) 337–345.
[18] A.P. Roberts, C.R. Pike, K.L. Verosub, First-order reversal curves: a new tool for characterizing the magnetic properties of natural samples, J. Geophys. Res. 105 (2000) 28461–28475.
[19] S. Cisowski, Interacting vs. non-interacting single-domain behaviour in natural and synthetic samples, Phys. Earth Planet. Inter. 26 (1981) 56–62.
[20] R.B. Frankel, J.P. Zhang, D.A. Bazylinski, Single magnetic domain in magnetotactic bacteria, J. Geophys. Res. 103 (1998) 30601–30604.
[21] D.J. Dunlop, Ö. Özdemir, Rock Magnetism: Fundamental and Frontiers, Cambridge University Press, Cambridge, 1997, 573 pp.
[22] A.V. Smirnov, J.A. Tarduno, Low-temperature magnetic properties of pelagic sediments (Ocean Drilling Program Site 805C): tracers of maghemitization and magnetic mineral reduction, J. Geophys. Res. 105 (2000) 16457–16471.
[23] B.P. Weiss, S.S. Kim, J.L. Kirschvink, R.E. Kopp, M. Sankaran, A. Kobayashi, A. Komeili, Ferromagnetic resonance and low-temperature magnetic tests for biogenic magnetite, Earth Planet. Sci. Lett. 224 (2004) 73–89.
[24] Ö. Özdemir, D.J. Dunlop, B.M. Moskowitz, Changes in remanence, coercivity and domain state at low temperature in magnetite, Earth Planet. Sci. Lett. 194 (2002) 343–358.
[25] A.R. Muxworthy, W. Williams, Micromagnetic models of pseudo-single domain grains of magnetite near the Verwey transition, J. Geophys. Res. 104 (1999) 29203–29218.
[26] W.F. Jaep, Anhysteretic magnetization of an assembly of single-domain particles, J. Appl. Phys. 40 (1969) 1297–1298.
[27] R.J. Veitch, Calculated anhysteretic susceptibility due to domain wall motion in two-domain magnetite spheres, Geophys. Res. Lett. 11 (1984) 181–184.
[28] N. Sugiura, ARM, TRM, and magnetic interactions: concentration dependence, Earth Planet. Sci. Lett. 42 (1979) 451–455.
[29] D.J. Dunlop, Coercive forces and coercivity spectra of submicron magnetites, Earth Planet. Sci. Lett. 78 (1986) 288–295.
[30] M. Hanzlik, M. Winklhofer, N. Petersen, Pulsed-field-remanence measurements on individual magnetotactic bacteria, J. Magn. Magn. Mater. 248 (2002) 258–267.
[31] A.R. Muxworthy, D. Heslop, W. Williams, Influence of magnetostatic interactions on first-order-reversal-curve (FORC) diagrams: a micromagnetic approach, Geophys. J. Int. 158 (2004) 888–897.
[32] H. Vali, B. Weiss, Y.L. Li, S.K. Sears, S.S. Kim, J.L. Kirschvink, C. Zhang, Formation of tabular single-domain magnetite induced by Geobacter metallireducens GS-15, Proc. Natl. Acad. Sci. 101 (2004) 16121–16126.
[33] R.P. Weiss, S.S. Kim, J.L. Kirschvink, R.E. Kopp, M. Sankaran, A. Kobayashi, A. Komeili, Magnetic tests for magnetosome chains in Martian meteorite ALH84001, Proc. Natl. Acad. Sci. 101 (2004) 8281–8284.
[34] Ö. Özdemir, D.J. Dunlop, B.M. Moskowitz, The effect of oxidation on the Verwey transition in magnetite, Geophys. Res. Lett. 20 (1993) 1671–1674.
[35] H. Vali, J.L. Kirschvink, Magnetofossil dissolution in a palaeomagnetically unstable deep-sea sediment, Nature 339 (1989) 203–206.
[36] K. Hilgenfeldt, Diagenetic dissolution of biogenic magnetite in surface sediments of the Benguela upwelling system, Int. J. Earth Sci. 88 (2000) 630–640.
[37] R. Egli, Characterization of individual rock magnetic components by analysis of remanence curves: 3. Bacterial magnetite and natural processes in lakes, Phys. Chem. Earth 29 (2004) 869–884.